Atmospheric
Chemistry
and Physics

Nucleation modeling of the Antarctic stratospheric CN layer and derivation of sulfuric acid profiles

Steffen Münch[1,a] **and Joachim Curtius**[1]

[1]Institute for Atmospheric and Environmental Sciences, Goethe University Frankfurt am Main,
60323 Frankfurt am Main, Germany
[a]now at: Institute for Atmospheric and Climate Science, ETH Zurich, 8092 Zurich, Switzerland

Correspondence to: Steffen Münch (steffen.muench@env.ethz.ch)

Abstract. Recent analysis of long-term balloon-borne measurements of Antarctic stratospheric condensation nuclei (CN) between July and October showed the formation of a volatile CN layer at 21–27 km altitude in a background of existing particles. We use the nucleation model SAWNUC to simulate these CN in subsiding air parcels and study their nucleation and coagulation characteristics. Our simulations confirm recent analysis that the development of the CN layer can be explained with neutral sulfuric acid–water nucleation and we show that outside the CN layer the measured CN concentrations are well reproduced just considering coagulation and the subsidence of the air parcels. While ion-induced nucleation is expected as the dominating formation process at higher temperatures, it does not play a significant role during the CN layer formation as the charged clusters recombine too fast. Further, we derive sulfuric acid concentrations for the CN layer formation. Our concentrations are about 1 order of magnitude higher than previously presented concentrations as our simulations consider that nucleated clusters have to grow to CN size and can coagulate with preexisting particles. Finally, we calculate threshold sulfuric acid profiles that show which concentration of sulfuric acid is necessary for nucleation and growth to observable size. These threshold profiles should represent upper limits of the actual sulfuric acid outside the CN layer. According to our profiles, sulfuric acid concentrations seem to be below midlatitude average during Antarctic winter but above midlatitude average for the CN layer formation.

1 Introduction

Atmospheric aerosol particles are of interest due to their various influences on radiation, clouds, chemistry, and air quality. Condensation nuclei counters measure the number concentration of aerosol particles by growing them to optically detectable sizes by condensation (e.g., McMurry, 2000). Therefore, condensation nuclei (CN) are defined as all aerosol particles that are large enough to be measured by a CN counter operating at a given supersaturation, which typically can measure particles with diameters larger than ~ 10 nm. New particle formation to supply the particles for the stratosphere mostly occurs in the tropical tropopause layer (Brock et al., 1995; Thomason and Peter, 2006; Weigel et al., 2011). The particles are then distributed in the lower stratosphere and constitute the stratospheric aerosol layer (Junge et al., 1961). The particles are sulfuric acid–water droplets (Arnold et al., 1998; Deshler, 2008; Junge et al., 1961), and if they are completely volatile, they are assumed to be formed by ion-induced or neutral homogeneous nucleation of sulfuric acid and water (binary nucleation). Binary nucleation occurs at low temperatures and high sulfuric acid concentrations. In the stratosphere the lowest temperatures are found in the polar vortex of the winter hemisphere. In the Antarctic polar vortex a background CN concentration of ~ 10 cm^{-3} is found (Campbell and Deshler, 2014). Volatility measurements indicate that more than half of them have a nonvolatile core which could be meteoric material (Campbell and Deshler, 2014; Curtius et al., 2005). Sulfuric acid is expected to condense on these CN (Borrmann et al., 2010; Murphy et al., 1998, 2014) and the formation rate of gaseous

sulfuric acid should be very small during polar night. Therefore, nucleation is not expected to occur in the polar vortex.

Contrary to this expectation, Rosen and Hofmann (1983) first observed an increase in volatile CN at 25–30 km altitude during winter at Laramie, Wyoming (41° N). They assumed the CN to be freshly nucleated sulfuric acid–water particles with the polar stratosphere as the source region. Above McMurdo Station, Antarctica (78° S), Hofmann and Rosen (1985) also observed an increased CN concentration between 20 and 25 km after sunrise (CN layer). To check if the occurrence of this CN layer was an annual polar phenomenon, further measurements were performed that also observed the formation of a CN layer after sunrise (e.g., Hofmann, 1990, at Kiruna, Sweden (68° N)). Therefore, sulfuric acid production by sunlight after the end of the polar night was suggested as the nucleation source.

Based on these observations, modeling studies began to investigate the formation of the CN layer. Hamill et al. (1990) calculated nucleation rates indicating that binary nucleation could occur in the polar winter stratosphere if sulfuric acid concentrations were high enough. Zhao et al. (1995) developed a one-dimensional (altitude) aerosol model that showed that the transformation of carbonyl sulfide (OCS) to SO_2 and further oxidation of SO_2 to sulfuric acid are too slow to reproduce the observed CN increase. They could only reproduce the formation of the CN layer when they added downward transport of SO_2 from the mesosphere inside the polar vortex. Mills et al. (1999, 2005) presented modeling with a two-dimensional (altitude and latitude) aerosol model that was able to reproduce the formation of the CN layer when including production of mesospheric SO_2 by photolysis of sulfuric acid and SO_3 (see also Vaida et al., 2003).

In summary, and contrary to the initial expectation, nucleation seems to occur in the polar stratosphere. During polar winter, more SO_2 is transported downward inside the polar vortex without being oxidized by photochemical reactions. After sunrise, this SO_2 is oxidized to sulfuric acid, which initiates nucleation and forms the volatile CN layer despite the presence of nonvolatile background CN.

More recently, Campbell and Deshler (2014) presented a long-term record of stratospheric balloon-borne CN measurements that were performed 2–3 times a year during winter from 1986 until 2010 above McMurdo Station, Antarctica (78° S). They present monthly averaged CN concentration and temperature profiles which capture the unperturbed CN, with concentrations around $10–20\,cm^{-3}$ in June/July as well as the development of the CN layer at 21–27 km, with concentrations increasing to $100\,cm^{-3}$ from August until October during sunrise and warming. Campbell and Deshler (2014) also presented volatility measurements of the CN showing that in general more than half of the CN have a nonvolatile core except in the CN layers where they observe significant and rapid formation of new particles that are completely volatile. Additionally, Campbell et al. (2014) used a three-dimensional chemistry climate model (English et al.,

2011; Hurrell et al., 2013) to reveal the global extent of the CN layer.

Campbell and Deshler (2014) describe a method where they derive an Antarctic sulfuric acid profile from the measured CN by inverting the neutral binary nucleation equation. They used the difference between the CN before sunrise and two weeks after sunrise averaged over all years to derive a nucleation rate for all altitudes from which they derived the corresponding sulfuric acid. This profile is useful, for example, for evaluating global models (Campbell et al., 2014) as no Antarctic sulfuric acid measurements exist. However, Campbell and Deshler (2014) and Campbell et al. (2014) also note that their derived profile might be an underestimation as their method does not consider the particles smaller than their experimental CN detection threshold particle size, losses to preexisting particles, and ion-induced nucleation.

We find this approach of deriving a sulfuric acid profile from the measured CN intriguing. Here we use the nucleation model SAWNUC that simulates small particles, ion-induced nucleation, coagulation, and losses to preexisting particles. We model the Antarctic CN layer based on the observations of Campbell and Deshler (2014) and derive Antarctic stratospheric sulfuric acid profiles.

2　Methods

2.1　The SAWNUC model

The SAWNUC (Sulfuric Acid Water NUCleation; Lovejoy et al., 2004) model simulates binary sulfuric acid water neutral and ion-induced nucleation. SAWNUC uses thermodynamic stabilities that are based on experimental values and quantum chemical calculations (Lovejoy and Curtius, 2001; Froyd and Lovejoy, 2003a, b; Hanson and Lovejoy, 2006), and it explicitly simulates step-by-step addition of sulfuric acid molecules in linear size bins for cluster sizes below 2 nm. Above 2 nm particle concentrations are collected in geometric size bins. Here we simulate 30 geometric size bins with a scale factor of 1.7, ranging up to about 400 nm for neutral and negatively charged clusters. For each size bin, SAWNUC can simulate condensation and evaporation of sulfuric acid, coagulation with neutral clusters, recombination of negative clusters with positive ions, and losses to preexisting particles. SAWNUC has been previously described and used (among others) by Lovejoy et al. (2004), Ehrhart and Curtius (2013), Kürten et al. (2015), Ehrhart et al. (2016), and its parameterized version, PARNUC (Kazil and Lovejoy, 2007), is used in Kirkby et al. (2011).

For this study, we extended the SAWNUC model. As in Kürten et al. (2015), coagulation rates between neutral clusters are now calculated including van der Waals forces according to Chan and Mozurkewich (2001). We redesigned the model code to allow for changes in ambient conditions during a simulation and added the ability to perform mul-
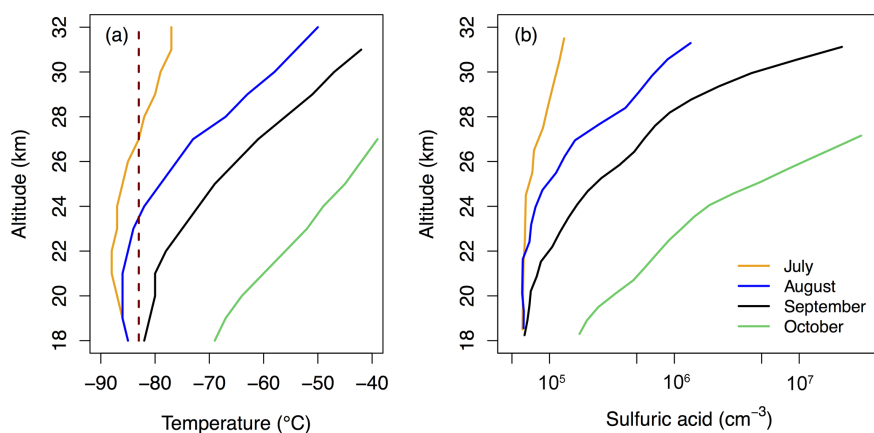
Figure 1. Temperatures **(a)** during Antarctic winter above McMurdo Station, Antarctica (78° S), as presented in Campbell and Deshler (2014). The dashed line shows the lower temperature limit for which the SAWNUC model is valid and at which lower temperatures were kept fixed. In **(b)**, corresponding sulfuric acid profiles are shown that lead to a 10 % CN increase by nucleation and growth to observable size during 1 month. For these *nucleation threshold profiles*, we assume a monodisperse CN background of $10 \, \mathrm{cm}^{-3}$ with 100 nm diameter at all altitudes (18–32 km) for every month (July–October).

tiple simulations within one program run. We do not use SAWNUC's procedure to represent losses to preexisting particles by a single surface area loss term, but instead we now fully simulate preexisting particles as initial particle concentrations. For this study, the basic processes simulated by SAWNUC are condensation and evaporation of sulfuric acid and coagulation for every size bin. Condensation and evaporation of sulfuric acid are the dominating processes for the formation of new particles, while coagulation and condensation of sulfuric acid, if present, determine growth and number reduction of existing particles.

2.2 Ambient parameters

To perform a regular SAWNUC simulation for a given region of the Antarctic stratosphere, the temperature, pressure, ion pair production rate, relative humidity, and sulfuric acid concentration are required. Particle concentrations and sizes are the model output at every time step. When inverting SAWNUC, the particle concentrations are required to derive the sulfuric acid concentrations.

Temperatures above Antarctica are taken from Campbell and Deshler (2014), and those temperatures that are below 190 K (maximum 5 K below), which is SAWNUC's lower limit of the temperature range, are fixed at 190 K. This introduces some uncertainty which is estimated in our sensitivity test of a 5 K temperature increase (Sect. 3.3). Altitudes are converted to pressures according to the global modeling of Campbell et al. (2014). The ionization rate of the Antarctic stratosphere in August–September 2010 was 3×10^5 ion pairs per gram of air and second (Ilya Usoskin, personal communication, 2013 according to Usoskin et al., 2011), which converts to, for example, ~ 10 ion pairs $\mathrm{cm}^{-3} \, \mathrm{s}^{-1}$ at 200 K and 20 hPa. The water vapor profile for July increases linearly

from 3.0 to 6.0 ppm between 18 and 25 km, while remaining at a constant value of 6.0 ppm up to 32 km based on the Microwave Limb Sounder (Waters et al., 2006) and hygrometer (Vömel et al., 1995) measurements in Fig. 7a in Campbell and Deshler (2014). The water vapor mixing ratio is kept constant during the subsidence of the simulated air parcels (see below).

CN concentrations are taken from Campbell and Deshler (2014). The measured CN are then compared with the simulated CN by summing over all simulated particles with diameters above 20 nm, as Campbell and Deshler (2014) reported a detection limit of their CN counters of 6–20 nm diameter. As we do not know the exact size of the measured CN, we assume the initial preexisting CN to have a diameter of 100 nm (see below), but we also perform sensitivity studies assuming different sizes in Sect. 3.3. We simulate them as pure sulfuric acid–water particles but as temperatures are too low for significant evaporation, they could also include a nonvolatile core.

3 Results

3.1 CN simulations and sulfuric acid profiles

We start our simulations with a simplified *reference case* where we assume for all altitudes (18–32 km) and for every month (July–October) a constant monodisperse background CN concentration of $10 \, \mathrm{cm}^{-3}$ with a diameter of 100 nm. For this reference case, we do not simulate the region above 31 km in September and above 27 km in October, as high temperatures lead to evaporation of the initial background CN and complicate the interpretation. For all other altitudes and months, we simulate 1 month with constant ambient conditions chosen according to Sect. 2.2. We use the tempera-
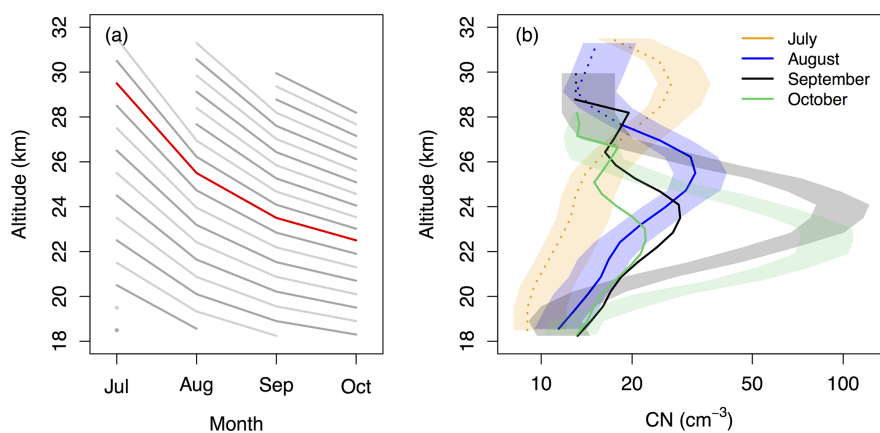
Figure 2. Air parcel subsidence trajectories **(a)** and simulated CN (monthly mean) without gaseous sulfuric acid being present **(b)**. The uncertainty ranges of the measured CN presented in Campbell and Deshler (2014) are shown as shaded areas in **(b)** for comparison. The trajectories of the simulated air parcels were placed around the subsidence of the measured CN maximum (red). In the simulation, the ambient conditions are kept constant during each month. For the first month of each trajectory, the CN concentrations (dotted) are chosen based on Campbell and Deshler (2014). In the following months, the simulated CN concentrations (solid) are the result of only coagulation and air volume compression, as there is no gaseous sulfuric acid present.
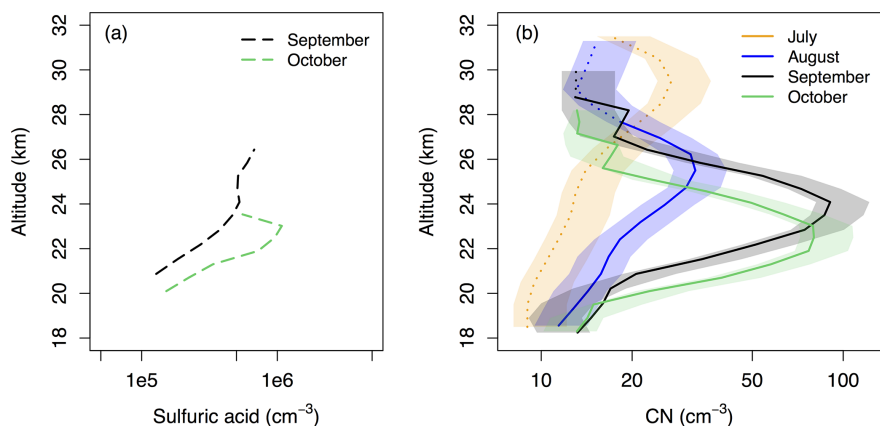

Figure 3. CN layer gaseous sulfuric acid profiles **(a)** and the simulated CN using these profiles **(b)**. We derive the sulfuric acid if the simulated CN concentrations in Fig. 2b are too low without gaseous sulfuric acid being present and therefore nucleation and condensational growth are needed to simulate the CN layer. As in Fig. 2b, the dotted lines are the initial CN based on observations and the solid lines are the simulated CN. The uncertainty ranges of the measured CN from Campbell and Deshler (2014) are shown as shaded areas for comparison.

tures reported by Campbell and Deshler (2014) which are reproduced in Fig. 1a. We set the background concentration of $10\,\mathrm{CN\,cm^{-3}}$ as initial particle concentrations at the beginning of the month and simulate the month without gaseous sulfuric acid being present. The CN concentration then reduces somewhat over time as the particles coagulate. Then, we simulate the month again and derive the gaseous sulfuric acid concentration that leads to a 10 % higher monthly mean CN concentration. This we term the *nucleation threshold profile* for sulfuric acid as it defines the minimum gaseous sulfuric acid that leads to nucleation and growth to observable CN size of about 1 additional CN per $\mathrm{cm^3}$ and month in a background of 10 preexisting $\mathrm{CN\,cm^{-3}}$. Note that even though the idealized assumption of zero gaseous sulfuric

acid is unphysical, it helps us to fully isolate and understand the processes that occur. All results of this study hardly change if we assume a minimum sulfuric acid concentration of $10^4\,\mathrm{cm^{-3}}$ instead of zero sulfuric acid. Although the $10^4\,\mathrm{cm^{-3}}$ sulfuric acid would be more realistic, we preferred the idealized choice of zero sulfuric acid to be able to completely decouple the processes.

The nucleation threshold sulfuric acid profiles are shown in Fig. 1b. Their shapes are similar to the temperature profiles because temperature, sulfuric acid, and losses to preexisting particles mainly determine the nucleation rate. As the preexisting particle concentrations are the same and we target almost the same nucleation rate everywhere, the temperature determines the derived sulfuric acid concentration, and the
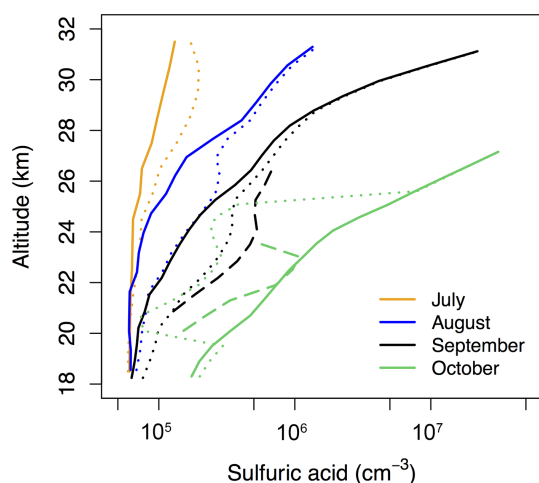
Figure 4. Combination of the nucleation threshold sulfuric acid profiles from Fig. 1b (solid) and the CN layer sulfuric acid profiles from Fig. 3a (dashed). Additionally, we show sulfuric acid profiles that cause a CN increase in our CN simulation of Fig. 3b (dotted) which should represent upper limits of the Antarctic winter stratospheric sulfuric acid outside the CN layer.

nucleation threshold profiles consequently increase with increasing temperature. However, the water vapor concentration also has a small influence on the derived profiles as can be seen, for example, in July below 27 km, where the temperature is fixed to 190 K but the derived profile still varies slightly.

We continue by studying how the measured CN of Campbell and Deshler (2014) coagulate outside the CN layer. Therefore, we drop the assumption of 10 CN cm^{-3} from the reference case and simulate the CN inside air parcels that subside in the polar vortex. The monthly average CN profiles presented in Fig. 1c in Campbell and Deshler (2014) are our basis for the air parcel subsidence trajectories. Campbell and Deshler (2014) suggested air subsidence inside the polar vortex as the explanation for the subsidence of the CN maximum from July to October. We follow their suggestion and assume that the CN maximum of each month resides in a single subsiding air parcel, and place the other air parcel trajectories around this CN maximum trajectory (Fig. 2a; description in Sect. S2 in the Supplement). Note that the CN maximum subsidence trajectory is an average over 24 years of measurements and therefore our air parcel trajectories represent idealized descents. The pathways outside the CN layer are just rough estimates. However, our trajectories seem reasonable as Hardiman et al. (2013) find residual vertical velocities of about 0.6 mm s^{-1} (≈ 1.5 km per month) at 80° S and 70 hPa that increase with height in their analysis of the Brewer–Dobson circulation in CMIP5 simulations. For an air parcel simulation, we set the ambient conditions at the beginning of each month according to Sect. 2.2 and keep them constant for the whole month. We simulate and compare the

values on a monthly basis as the measured input and target values (temperature and CN) are monthly averages as well. For the first month of each parcel simulation, we use the measurements of Campbell and Deshler (2014) to determine the initial CN concentration and subsequently simulate this month. As we still assume no gaseous sulfuric acid being present, coagulation is the only process taking place which reduces the CN by some amount. We choose the initial CN concentration so that the mean CN concentration in the first month matches the measurements. After the first month, we let the model run free, still assuming zero gaseous sulfuric acid. Therefore, the only two effects on CN concentration are a decrease due to coagulation and an increase when the ambient conditions change between the months. The latter results from an air volume expansion by temperature increase and an air volume compression by pressure increase which is mostly dominated by the pressure effect and consequently results in a net CN concentration increase.

Figure 2b shows the simulated CN without sulfuric acid being present and therefore no nucleation. The uncertainty ranges of the measured CN from Campbell and Deshler (2014) are shown for comparison (-10 to $+35$ %). As the first value of every simulated air parcel is chosen based on the observations, the CN in July and at the top in August and September are identical with the measurements (dotted). In the following months, the CN result from our simulation (solid). In August, subsidence and air compression of the July CN dominate over coagulation throughout the simulated profile and lead to higher CN concentrations. Thereby, the measured CN can be fully reproduced within the uncertainty range without nucleation of new particles being necessary. In September and October, the modeled CN concentrations at 20–27 km are too small under a zero gaseous sulfuric acid condition, and the CN layer is not simulated.

In September, above the CN layer at ~ 28 km, too many CN are simulated even without any gaseous sulfuric acid being present (Fig. 2b). This is the result of an air volume compression in the subsiding air parcels from 31 km in August to 28 km in September which increases the CN concentration by ~ 60 %. Here, coagulation is not efficient enough to reduce the monthly mean CN to the observed value. The high October CN at ~ 26.5 km are then a result of the high September values. If the August CN concentration at ~ 31 km is reduced by about one-third, the simulated CN in September and October would be within the measurement range.

It is important to understand how much sulfuric acid is necessary to form the CN layer, and thus reproduce the observations. Using the same method as before, we now derive the amount of sulfuric acid needed to match the simulated and measured CN. This sulfuric acid causes nucleation of new particles, growth of these new particles to CN size, and growth of existing CN.

Figure 3a shows the sulfuric acid profiles that are necessary to form the CN layer and reproduce the observations (termed "*CN layer profiles*"). Sulfuric acid is needed

in September at 21–26 km to form the CN layer and in October at 20–24 km to prevent the CN layer from decreasing too fast by coagulation. Figure 3b shows the simulated CN using the derived sulfuric acid profiles, and as expected the measured CN profiles are reproduced for all months at almost all altitudes.

For a complete interpretation of the processes in the CN layer we combine our nucleation threshold profiles and CN layer profiles in Fig. 4 (solid and dashed). Additionally, we derive the sulfuric acid concentrations that lead to a CN increase in our simulation of the observed CN (Fig. 3b) and include them in Fig. 4 (dotted). We use the same method as for our nucleation threshold profiles (deriving the amount of sulfuric acid that leads to a 10 % CN increase), but now with the simulated CN as background. Note that outside of the CN layer, these profiles represent only *upper limits* for the gaseous sulfuric acid in the atmosphere as neither the observations nor our simulations indicate nucleation in these areas.

In July, August, and September, the upper limit profiles (dotted) show the sulfuric acid that is necessary for nucleation and growth to CN size and leads to additional 10 % CN within 1 month. The concentrations are higher than our nucleation threshold profiles (solid) because we have a higher concentration of preexisting CN compared to the $10 \, \text{cm}^{-3}$ in the reference case. Therefore, more small clusters are lost by coagulation with large CN. Here nucleation is in competition with losses to preexisting particles (Ehrhart and Curtius, 2013). In September, the sulfuric acid profile that forms the CN layer (dashed) has higher concentrations than both the nucleation profile (solid) and the upper limit profile (dotted). This means that new particles are nucleating and that more than the 10 % additional CN of the upper limit case have to form. However, as the nucleation rate is very sensitive to changes in sulfuric acid, the derived CN layer sulfuric acid concentrations are not much higher than the upper limit concentrations.

In October in the area of the CN layer, however, the upper limit profile (dotted) and the CN layer formation profile (dashed) are both lower than the nucleation profile (solid), showing that no new particles have to nucleate. Instead, small particles that still exist from the nucleation event in September can grow above the CN counting threshold, which requires less sulfuric acid than nucleation and growth of new CN. Therefore, the history of the nucleation event in September allows for a CN increase without new particle formation in October.

In the following sensitivity studies we show and discuss only the nucleation threshold and the CN layer profiles to avoid overloaded figures, but the conclusions for the upper limit profiles are analogous to the other profiles.

3.2 Ion-induced nucleation

Figure 5 shows the impacts of ion-induced nucleation on the derived sulfuric acid profiles by removing all ions from the
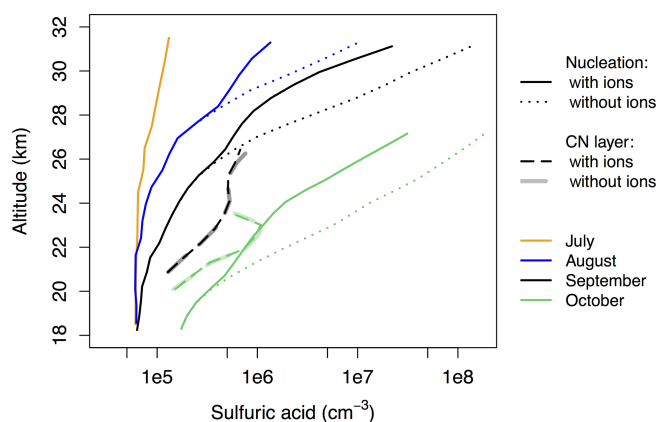

Figure 5. Comparison of the nucleation threshold sulfuric acid profiles derived including ion-induced nucleation (solid lines) and without simulating ions (dotted lines). At low sulfuric acid concentrations the derived profiles do not change. The CN layer profiles also hardly change (thick dashed lines; grey and light green are without ions and black and green are with ions, but they are almost identical).

simulations and then comparing the derived profiles to those that included ions. In areas with low sulfuric acid concentrations, removing the ions has nearly no effect on the derived profiles; however, in areas with higher sulfuric acid concentrations the derived profiles increase by almost an order of magnitude. At low sulfuric acid concentrations, the small clusters are not growing fast enough by condensation. Negatively charged clusters recombine too early with positively charged ions and therefore are too small to overcome the nucleation barrier of neutral nucleation. At higher sulfuric acid concentrations, ion-induced nucleation occurs as expected. The charged clusters grow larger than the critical size before they recombine and increase the nucleation rate. Thus to create the same number of CN without ions, more sulfuric acid is required than if ions are present.

For the nucleation threshold profiles with $10 \, \text{cm}^{-3}$ background CN, ion-induced nucleation starts to occur at sulfuric acid concentrations of $\sim 4 \times 10^5 \, \text{cm}^{-3}$. During the formation of the CN layer, however, there are more preexisting CN present that reduce the nucleation efficiency and therefore ion-induced nucleation only starts to occur at sulfuric acid concentrations of $\sim 6 \times 10^5 \, \text{cm}^{-3}$. As the derived sulfuric acid concentrations are below that limit in September, the CN layer formation is not influenced significantly by ion-induced nucleation. In October, the CN layer is located mostly in the area where ions do change the nucleation rates, but as there is no nucleation of new particles during that time, the derived sulfuric acid hardly changes by ion-induced nucleation.

3.3 Sensitivity studies

To study the uncertainty introduced by the assumed particle size threshold of the CN measurements, we derive the sulfu-
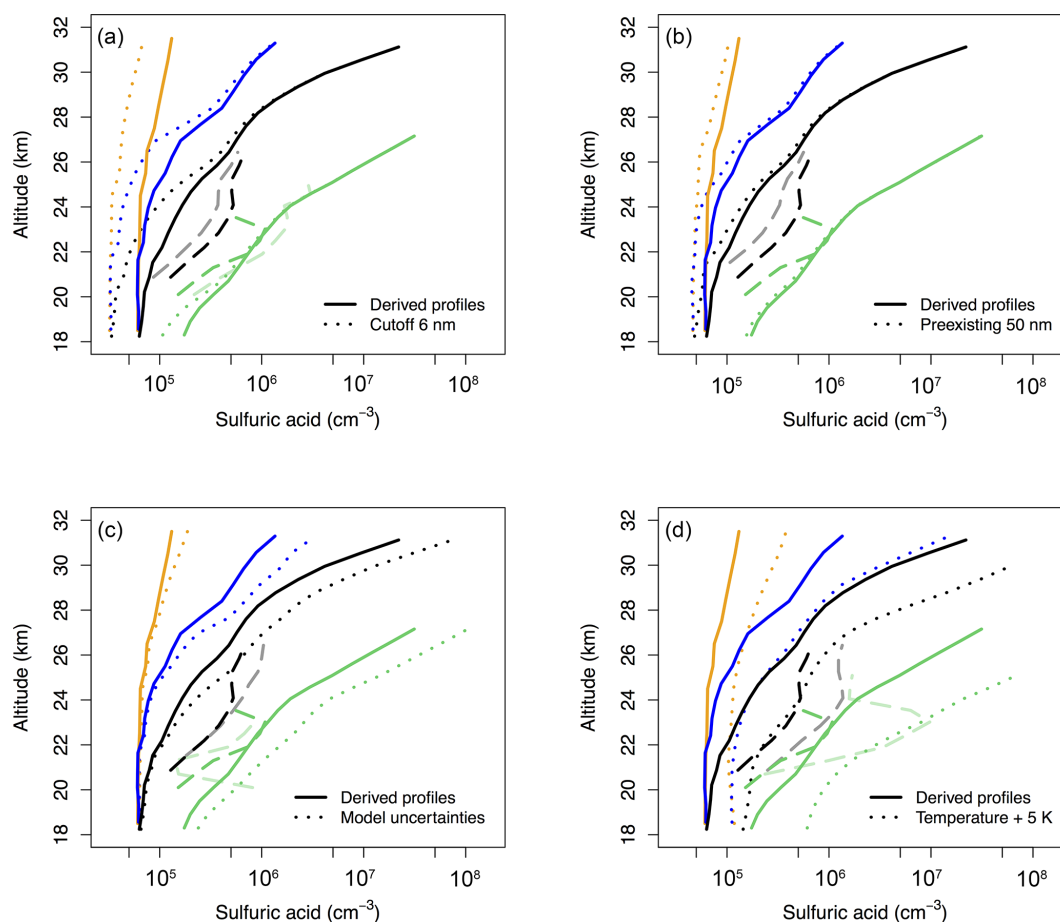
Figure 6. Sensitivity studies varying **(a)** CN counter cutoff size, **(b)** preexisting particle size, **(c)** model thermochemical and dynamic parameters, and **(d)** temperature to estimate the uncertainties of the derived sulfuric acid profiles. As in Fig. 5, the solid and dark dashed lines show the nucleation threshold and CN layer formation profiles as presented in Fig. 4. The dotted and light dashed lines show the changed profiles according to the sensitivity tests.

ric acid profiles assuming a lower CN counter threshold of 6 nm diameter, which is the CN counter's lower end according to Campbell and Deshler (2014). The lower threshold leads to lower sulfuric acid concentrations as the nucleated CN do not have to grow as large by sulfuric acid condensation to be counted (Fig. 6a). The impact of CN threshold size decreases with increasing sulfuric acid as, at higher concentrations, the clusters grow quickly once they are nucleated. In October, however, there is more sulfuric acid needed in the CN layer as fewer small clusters exist that can grow across the cutoff size and therefore some nucleation of new CN is needed.

Lowering the size of the initial preexisting particles from 100 to 50 nm diameter reduces their coagulation efficiency and they present a smaller loss during nucleation. Therefore, the modeled sulfuric acid concentrations are lower (Fig. 6b). For the same reason there is no sulfuric acid needed in October in the CN layer. If we assume the initial preexisting particles to be a distribution of different sizes (e.g., 40 % of

50 nm, 50 % of 100 nm, and 10 % of 300 nm particles), the coagulation efficiency increases and leads to fewer simulated CN and higher derived sulfuric acid profiles (Fig. S1 in the Supplement).

We study model uncertainties according to Lovejoy et al. (2004) by adding 0.5 kcal to all changes in Gibbs free energy of negatively charged clusters. This only increases the profiles in regions where ion-induced nucleation dominates (see Sect. 3.2 and Fig. 5). A reduction of all coagulation and condensation rates by 20 % increases all profiles a little but leads to a poorer CN simulation in comparison with the observations. The updated neutral sulfuric acid dimer thermodynamic stabilities presented by Kürten et al. (2015), which have a higher relative humidity dependence of the equilibrium constant, lead to higher dimer evaporation rates. Therefore, they increase our profiles at low relative humidities (high temperatures), but only if neutral binary nucleation dominates. A combination of these influences is shown in Fig. 6c. The increase in the September CN layer profile at
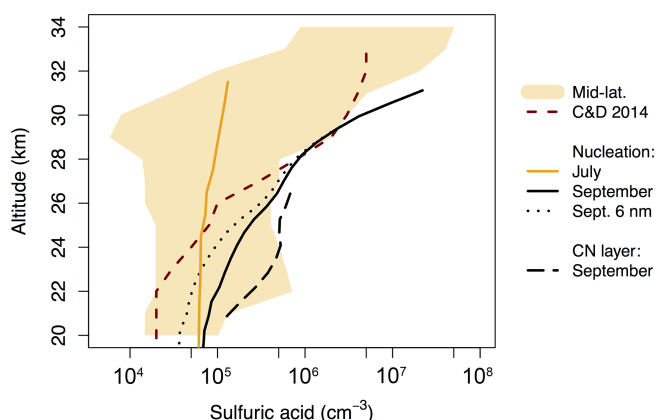
Figure 7. Comparison of our derived Antarctic sulfuric acid profiles (nucleation threshold: solid; CN layer: long dashed) with the derived profile from Campbell and Deshler (2014) (dark red, short dashed) and midlatitude measurements and modeling of Arnold et al. (1981), Reiner and Arnold (1997), Schlager and Arnold (1987), Viggiano and Arnold (1981), and Mills et al. (2005) (shaded area). The September nucleation threshold profile for nucleation and growth to a lower cutoff of 6 nm from Fig. 6a is also included (black dotted).

24–26 km is mainly due to the updated dimer thermodynamic stabilities. The October CN layer profile mostly decreases as coagulation is less efficient, which requires less growth of additional small particles. At the lowest altitude no nucleation is needed in September, but therefore nucleation of additional CN is necessary in October.

As the derived sulfuric acid profiles are mainly determined by temperature we also test the effect of a 5 K temperature increase (Fig. 6d). We removed the responses at the highest September and October values as there the temperature was too high, so that evaporating particles complicate the situation. A 5 K temperature increase significantly increases the sulfuric acid profiles by a factor of 2 in the coldest regions and up to a factor of 15 in the warmest regions. Fortunately, the temperature measurement uncertainty is only 0.5 K (Campbell and Deshler, 2014). However, this temperature sensitivity shows that our sulfuric acid profiles in July and August at low altitudes are up to a factor of 2 too high as there we had to increase the temperature to SAWNUC's lower temperature limit of 190 K (maximum increase of 5 K; see Fig. 1a).

Our trajectories might descend too fast from July to August as the CN profile of Campbell and Deshler (2014) is representative of June and July. Also, Campbell and Deshler (2014) note that most measurements were performed between late August and early October, while our October simulations reproduce the measured CN as a monthly mean. If we run our simulations from mid-June until mid-October, the simulated CN in August are lower as the preexisting CN have more time to coagulate and in October less sulfuric acid is necessary to reproduce the CN layer (Fig. S2). Note that, in

combination with a preexisting particle size distribution, this might necessitate some nucleation already in August.

Additional sensitivity studies (Fig. S3) imply that the exact number of ions or water molecules (e.g., 5 ppm everywhere) has only a small influence on the derived profiles because the ion concentrations are high enough that they are not a limiting factor, and the few parts per million stratospheric water vapor uncertainty is too small to influence the profiles significantly. Also, a formation of 35 % more CN in the layer (CN measurement uncertainty) needs only little additional sulfuric acid (not shown).

3.4 Comparison with midlatitude sulfuric acid and the derived profile of Campbell and Deshler (2014)

In Fig. 7 we compare our derived September CN layer sulfuric acid profile with the profile derived by Campbell and Deshler (2014). Campbell and Deshler (2014) derived sulfuric acid concentrations for 15 to 33 km (dark red, dashed). Our derived sulfuric acid (black, dashed) is only shown between 21 and 26 km as we need no nucleation above and below the CN layer to reproduce the observations. Our concentrations are about 1 order of magnitude higher. This is because our CN have to form in a background of preexisting particles and they have to grow to observable size. As our sensitivity tests show, both of these effects require more sulfuric acid. In the nucleation threshold profile with a cutoff of 6 nm and a background of $10 \, \mathrm{CN \, cm^{-3}}$ (black, dotted) these two effects are less pronounced, and therefore this profile compares better with the derived profile of Campbell and Deshler (2014).

We cannot compare our derived sulfuric acid profiles with Antarctic in situ or remote sensing measurements as such data do not exist to our knowledge. However, northern midlatitude balloon-borne measurements mainly from September and October have been published (Arnold et al., 1981; Reiner and Arnold, 1997; Schlager and Arnold, 1987; Viggiano and Arnold, 1981) and summarized by Mills et al. (2005). Note that due to the different tropopause heights (43° N vs. 78° S) our derived profiles might need to be shifted upwards for comparison. In July and August our nucleation threshold profiles lie within the midlatitude values. However, as nucleation does not occur, these profiles represent upper limits and Antarctic winter sulfuric acid concentrations are lower than average midlatitude concentrations. In September our derived sulfuric acid concentrations in the CN layer are higher than average midlatitude concentrations. This comparison supports the formation explanation of the CN layer with low sulfuric acid during Antarctic winter followed by an area of high sulfuric acid after sunrise.

We did not derive sulfuric acid profiles above Wyoming according to Fig. 1a and b of Campbell and Deshler (2014), as these CN are assumed to have nucleated in the polar region. However, as temperature mainly controls the nucleation rate, the nucleation threshold sulfuric acid profiles at tem-

peratures representative of the stratosphere above Wyoming are used for comparison. In autumn, temperatures above Wyoming lie between $-60°$ C at 17 km and $-40°$ C at 34 km (Campbell and Deshler, 2014, Fig. 1b). The same temperature range is found over Antarctica in September between 27 and 33 km (Campbell and Deshler, 2014, Fig. 1d). If we compare our September nucleation threshold profile (black, solid) between 27 and 33 km with the midlatitude values, we see that at all midlatitude altitudes the concentrations are just below our nucleation threshold values. This suggests that nucleation usually does not occur in the midlatitude stratosphere in this altitude range. Sometimes at the highest sulfuric acid levels, however, ion-induced nucleation may become efficient.

4 Summary and conclusions

Analysis of over 20 years (1986–2010) of balloon-borne stratospheric CN measurements above McMurdo Station, Antarctica, between July and October reveals the formation of a layer of mainly volatile CN at 21–27 km altitude in a background of preexisting particles (Campbell and Deshler, 2014). Here, we use the nucleation box model SAWNUC to simulate these CN in subsiding air parcels and study the nucleation processes.

The observed CN of Campbell and Deshler (2014) are reproduced by simulating subsiding air parcels with volume compression, coagulation, nucleation, and growth processes. Antarctic CN concentrations outside the CN layer can be explained by coagulation if air volume compression due to air parcel subsidence is considered. Neutral sulfuric acid–water nucleation forms the CN layer in September, while in October growth of small particles maintains the layer. Ion-induced nucleation does not occur at significant levels as sulfuric acid concentrations are too low and charged clusters recombine too fast. Our results complement Campbell and Deshler (2014), who showed that the CN decrease above Laramie, Wyoming, can be explained by coagulation and that almost all CN inside the CN layer are volatile and therefore can be explained by binary nucleation.

Sulfuric acid concentrations in September during the CN layer formation range from 1×10^5 cm^{-3} at 21 km to 6×10^5 cm^{-3} at 26 km, which is about 1 order of magnitude higher than the concentrations derived by Campbell and Deshler (2014). Our sensitivity tests show that more sulfuric acid is needed in our simulations because nucleated clusters have to grow to the CN counter's threshold size for detection and can coagulate with preexisting particles. Therefore, we can confirm the suggestion of Campbell and Deshler (2014) that their profiles might be an underestimation due to these effects.

Finally, we derived gaseous sulfuric acid profiles that show which concentration would be necessary for nucleation and growth to CN size to occur, which should represent upper limits of the actual sulfuric acid outside of the CN layer where neither the observations nor our simulations indicate nucleation to occur. The upper limits start at 18 km at concentrations below 10^5 cm^{-3} and increase to about 10^5 cm^{-3} in July, 10^6 cm^{-3} in August, and 10^7 cm^{-3} in September at 32 km, while in October they start at 2×10^5 cm^{-3} at 18 km and increase above 10^7 cm^{-3} at 27 km. According to these upper limits, sulfuric acid concentrations seem to be below midlatitude average during Antarctic winter but above midlatitude average during the CN layer formation, while midlatitude sulfuric acid concentrations in general seem to be too low for nucleation to occur. This is also in agreement with Campbell and Deshler (2014) and other seminal references contained within, who suggest that the midlatitude CN layer originally formed in the polar region.

If stratospheric sulfuric acid increases above our upper limits, e.g., because of volcanic eruptions or geoengineering, nucleation could occur. In the midlatitudes and in some relatively warm areas above Antarctica, this nucleation would be dominated by ion-induced nucleation and therefore would require less sulfuric acid than predicted by neutral binary nucleation theory. Note, however, that our upper limits would increase if there were more preexisting particles present.

In conclusion, our study supports the explanation of the CN layer as presented by Campbell and Deshler (2014). We can reproduce the CN that decrease over time by coagulation in a low sulfuric acid environment during Antarctic winter. In September between 21 and 26 km we can reproduce the observed CN layer only if we assume a higher sulfuric acid concentration that produces volatile CN mainly by neutral binary nucleation.

The Supplement related to this article is available online at https://doi.org/10.5194/acp-17-7581-2017-supplement.

References

Arnold, F., Fabian, R., and Joos, W.: Measurements of the height variation of sulfuric acid vapor concentrations in the stratosphere. Geophys. Res. Lett., 8, 293–296, 1981.

Arnold, F., Curtius, J., Spreng, S., and Deshler, T.: Stratospheric aerosol sulfuric acid: First direct in situ measurements using a novel balloon-based mass spectrometer apparatus, J. Atmos. Chem., 30, 3–10, 1998.

Borrmann, S., Kunkel, D., Weigel, R., Minikin, A., Deshler, T., Wilson, J. C., Curtius, J., Volk, C. M., Homan, C. D., Ulanovsky, A., Ravegnani, F., Viciani, S., Shur, G. N., Belyaev, G. V., Law, K. S., and Cairo, F.: Aerosols in the tropical and subtropical UT/LS: in-situ measurements of submicron particle abundance and volatility, Atmos. Chem. Phys., 10, 5573–5592, https://doi.org/10.5194/acp-10-5573-2010, 2010.

Brock, C. A., Hamill, P., Wilson, J. C., Jonsson, H. H., and Chan, K. R.: Particle formation in the upper tropical troposphere: A source of nuclei for the stratospheric aerosol, Science, 270, p. 1650, 1995.

Campbell, P. and Deshler, T.: Condensation nuclei measurements in the midlatitude (1982–2012) and Antarctic (1986–2010) stratosphere between 20 and 35 km, J. Geophys. Res.-Atmos., 119, 137–152, 2014.

Campbell, P., Mills, M., and Deshler, T.: The global extent of the mid stratospheric CN layer: A three-dimensional modeling study, J. Geophys. Res.-Atmos., 119, 1010–1030, 2014.

Chan, T. W. and Mozurkewich, M.:. Measurement of the coagulation rate constant for sulfuric acid particles as a function of particle size using tandem differential mobility analysis, J. Aerosol Sci., 32, 321–339, 2001.

Curtius, J., Weigel, R., Vössing, H.-J., Wernli, H., Werner, A., Volk, C.-M., Konopka, P., Krebsbach, M., Schiller, C., Roiger, A., Schlager, H., Dreiling, V., and Borrmann, S.: Observations of meteoric material and implications for aerosol nucleation in the winter Arctic lower stratosphere derived from in situ particle measurements, Atmos. Chem. Phys., 5, 3053–3069, https://doi.org/10.5194/acp-5-3053-2005, 2005.

Deshler, T.: A review of global stratospheric aerosol: Measurements, importance, life cycle, and local stratospheric aerosol, Atmos. Res., 90, 223–232, 2008.

Ehrhart, S. and Curtius, J.: Influence of aerosol lifetime on the interpretation of nucleation experiments with respect to the first nucleation theorem, Atmos. Chem. Phys., 13, 11465–11471, https://doi.org/10.5194/acp-13-11465-2013, 2013.

Ehrhart, S., Ickes, L., Almeida, J., Amorim, A., Barmet, P., Bianchi, F., Dommen, J., Dunne, E. M., Duplissy, J., Franchin, A., Kangasluoma, J., Kirkby, J., Kürten, A., Kupc, A., Lehtipalo, K., Nieminen, T., Riccobono, F., Rondo, L., Schobesberger, S., Steiner, G., Tomé, A., Wimmer, D., Baltensperger, U., Wagner, P. E., and Curtius, J.: Comparison of the SAWNUC model with CLOUD measurements of sulphuric acid-water nucleation, J. Geophys. Res.-Atmos., 121, https://doi.org/10.1002/2015JD023723, 2016.

English, J. M., Toon, O. B., Mills, M. J., and Yu, F.: Microphysical simulations of new particle formation in the upper troposphere and lower stratosphere, Atmos. Chem. Phys., 11, 9303–9322, https://doi.org/10.5194/acp-11-9303-2011, 2011.

Froyd, K. D. and Lovejoy, E. R.: Experimental thermodynamics of cluster ions composed of H_2SO_4 and H_2O. 2. Measurements

and ab initio structures of negative ions, J. Phys. Chem. A, 107, 9812–9824, 2003a.

Froyd, K. D. and Lovejoy, E. R.: Experimental thermodynamics of cluster ions composed of H_2SO_4 and H_2O. 1. Positive ions, J. Phys. Chem. A, 107, 9800–9811, 2003b.

Hamill, P., Toon, O. B., and Turco, R. P.: Aerosol nucleation in the winter Arctic and Antarctic stratospheres, Geophys. Res. Lett., 17, 417–420, 1990.

Hanson, D. R. and Lovejoy, E. R.: Measurement of the thermodynamics of the hydrated dimer and trimer of sulfuric acid, J. Phys. Chem. A, 110, 9525–9528, 2006.

Hardiman, S. C., Butchart, N., and Calvo, N.: The morphology of the Brewer–Dobson circulation and its response to climate change in CMIP5 simulations, Q. J. Roy. Meteor. Soc., 140, 1958–1965, 2014.

Hofmann, D. J.: Measurement of the condensation nuclei profile to 31 km in the Arctic in January 1989 and comparisions with Antarctic measurements, Geophys. Res. Lett., 17, 357–360, 1990.

Hofmann, D. J. and Rosen, J. M.: Antarctic observations of stratospheric aerosol and high altitude condensation nuclei following the El Chichon eruption, Geophys. Res. Lett., 12, 13–16, 1985.

Hurrell, J. W., Holland, M. M., Gent, P. R., Ghan, S., Kay, J. E., Kushner, P. J., Lamarque, J.-F., Large, W. G., Lawrence, D., Lindsay, K., Lipscomb, W. H., Long, M. C., Mahowald, N., Marsh, D. R., Neale, R. B., Rasch, P., Vavrus, S., Vertenstein, M., Bader, D., Collins, W. D., Hack, J. J., Kiehl, J., and Marshall, S.: The community earth system model: A framework for collaborative research, B. Am. Meteorol. Soc., 94, 1339–1360, 2013.

Junge, C. E., Chagnon, C. W., and Manson, J. E.: Stratospheric aerosols, J. Meteorol., 18, 81–108, 1961.

Kazil, J. and Lovejoy, E. R.: A semi-analytical method for calculating rates of new sulfate aerosol formation from the gas phase, Atmos. Chem. Phys., 7, 3447–3459, https://doi.org/10.5194/acp-7-3447-2007, 2007.

Kirkby, J., Kirkby, J., Curtius, J., Almeida, J., Dunne, E., Duplissy, J., Ehrhart, S., Franchin, A., Gagné, S., Ickes, L., Kürten, A., Kupc, A., Metzger, A., Riccobono, F., Rondo, L., Schobesberger, S., Tsagkogeorgas, G., Wimmer, D., Amorim, A., Bianchi, F., Breitenlechner, M., David, A., Dommen, J., Downard, A., Ehn, M., Flagan, R. C., Haider, S., Hansel, A., Hauser, D., Jud, W., Junninen, H., Kreissl, F., Kvashin, A., Laaksonen, A., Lehtipalo, K., Lima, J., Lovejoy, E. R., Makhmutov, V., Mathot, S., Mikkilä, J., Minginette, P., Mogo S., Nieminen, T., Onnela, A., Pereira, P., Petäjä, T., Schnitzhofer, R., J. H. Seinfeld, Sipilä, M., Stozhkov, Y., Stratmann, F., Tomé, A., Vanhanen, J., Viisanen, Y., Vrtala, A., Wagner, P. E., Walther, H., Weingartner, E., Wex, H., Winkler, P. M., Carslaw, K. S., Worsnop, D. R., Baltensperger, U., and Kulmala, M.: Role of sulphuric acid, ammonia and galactic cosmic rays in atmospheric aerosol nucleation, Nature, 476, 429–433, 2011.

Kürten, A., Münch, S., Rondo, L., Bianchi, F., Duplissy, J., Jokinen, T., Junninen, H., Sarnela, N., Schobesberger, S., Simon, M., Sipilä, M., Almeida, J., Amorim, A., Dommen, J., Donahue, N. M., Dunne, E. M., Flagan, R. C., Franchin, A., Kirkby, J., Kupc, A., Makhmutov, V., Petää, T., Praplan, A. P., Riccobono, F., Steiner, G., Tomé, A., Tsagkogeorgas, G., Wagner, P. E., Wimmer, D., Baltensperger, U., Kulmala, M., Worsnop,

D. R., and Curtius, J.: Thermodynamics of the formation of sulfuric acid dimers in the binary (H_2SO_4–H_2O) and ternary (H_2SO_4–H_2O–NH_3) system, Atmos. Chem. Phys., 15, 10701–10721, https://doi.org/10.5194/acp-15-10701-2015, 2015.

Lovejoy, E. R. and Curtius, J.: Cluster ion thermal decomposition (II): Master equation modeling in the low-pressure limit and fall-off regions. Bond energies for HSO_4-(H_2SO_4) x (HNO_3) y, J. Phys. Chem. A, 105, 10874–10883, 2001.

Lovejoy, E. R., Curtius, J., and Froyd, K. D.: Atmospheric ion-induced nucleation of sulfuric acid and water, J. Geophys. Res.-Atmos., 109, https://doi.org/10.1029/2003JD004460, 2004.

McMurry, P. H.: The history of condensation nucleus counters, Aerosol Sci. Tech., 33, 297–322, 2000.

Mills, M. J., Toon, O. B., and Solomon, S.: A 2D microphysical model of the polar stratospheric CN layer, Geophys. Res. Lett., 26, 1133–1136, 1999.

Mills, M. J., Toon, O. B., Vaida, V., Hintze, P. E., Kjaergaard, H. G., Schofield, D. P., and Robinson, T. W.: Photolysis of sulfuric acid vapor by visible light as a source of the polar stratospheric CN layer, J. Geophys. Res.-Atmos., 110, https://doi.org/10.1029/2004JD005519, 2005.

Murphy, D. M., Thomson, D. S., and Mahoney, M. J.: In situ measurements of organics, meteoritic material, mercury, and other elements in aerosols at 5 to 19 kilometers. Science, 282, 1664–1669, 1998.

Murphy, D. M., Froyd, K. D., Schwarz, J. P., and Wilson, J. C.: Observations of the chemical composition of stratospheric aerosol particles, Q. J. Roy. Meteor. Soc., 140, 1269–1278, 2014.

Reiner, T. and Arnold, F.: Stratospheric SO_3: Upper limits inferred from ion composition measurements-Implications for H_2SO_4 and aerosol formation, Geophys. Res. Lett., 24, 1751–1754, 1997.

Rosen, J. M. and Hofmann, D. J.: Unusual behavior in the condensation nuclei concentration at 30 km, J. Geophys. Res.-Oceans, 88, 3725–3731, 1983.

Schlager, H. and Arnold, F.: Balloon-borne composition measurements of stratospheric negative ions and inferred sulfuric acid vapor abundances during the MAP/GLOBUS 1983 campaign, Planet. Space Sci., 35, 693–701, 1987.

Thomason, L. and Peter, T.: SPARC assessment of stratospheric aerosol properties, WCRP-124, WMO/TD-No. 1295 (No. 4), SPARC Report, 2006.

Usoskin, I. G., Bazilevskaya, G. A., and Kovaltsov, G. A.: Solar modulation parameter for cosmic rays since 1936 reconstructed from ground-based neutron monitors and ionization chambers, J. Geophys. Res.-Space, 116, https://doi.org/10.1029/2010JA016105, 2011.

Vaida, V., Kjaergaard, H. G., Hintze, P. E., and Donaldson, D. J.: Photolysis of sulfuric acid vapor by visible solar radiation, Science, 299, 1566–1568, 2003.

Viggiano, A. A. and Arnold, F.: Extended sulfuric acid vapor concentration measurements in the stratosphere, Geophys. Res. Lett., 8, 583–586, 1981.

Vömel, H., Oltmans, S. J., Hofmann, D. J., Deshler, T., and Rosen, J. M.: The evolution of the dehydration in the Antarctic stratospheric vortex, J. Geophys. Res.-Atmos., 100, 13919–13926, 1995.

Waters, J. W., Froidevaux, L., Harwood, R. S., Jarnot, R. F., Pickett, H. M., Read, W. G., Siegel, P. H., Cofield, R. E., Filipiak, M. J., Flower, D. A., Holden, J. R., Lau, G. K., Livesey, N. J., Manney, G. L., Pumphrey, H. C., Santee, M. L., Wu, D. L., Cuddy, D. T., Lay, R. R., Loo, M. S., Perun, V. S., Schwartz, M. J., Stek, P. C., Thurstans, R. P., Boyles, M. A., Chandra, K. M., Chavez, M. C., Chen, G.-S., Chudasama, B. V., Dodge, R., Fuller, R. A., Girard, M. A., Jiang, J. H., Jiang, Y., Knosp, B. W., LaBelle, R. C., Lam, J. C., Lee, K. A., Miller, D., Oswald, J. E., Patel, N. C., Pukala, D. M., Quintero, O., Scaff, D. M., Van Snyder, W., Tope, M. C., Wagner, P. A., and Walch, M. J.: The earth observing system microwave limb sounder (EOS MLS) on the Aura satellite, IEEE T. Geosci. Remote Sens., 44, 1075–1092, 2006.

Weigel, R., Borrmann, S., Kazil, J., Minikin, A., Stohl, A., Wilson, J. C., Reeves, J. M., Kunkel, D., de Reus, M., Frey, W., Lovejoy, E. R., Volk, C. M., Viciani, S., D'Amato, F., Schiller, C., Peter, T., Schlager, H., Cairo, F., Law, K. S., Shur, G. N., Belyaev, G. V., and Curtius, J.: In situ observations of new particle formation in the tropical upper troposphere: the role of clouds and the nucleation mechanism, Atmos. Chem. Phys., 11, 9983–10010, https://doi.org/10.5194/acp-11-9983-2011, 2011.

Zhao, J., Toon, O. B., and Turco, R. P.: Origin of condensation nuclei in the springtime polar stratosphere, J. Geophys. Res.-Atmos., 100, 5215–5227, 1995.